CrystEngComm

Cite this: *CrystEngComm*, 2011, **13**, 2289

www.rsc.org/crystengcomm

PAPER

SnO_2 nanoribbons: excellent field-emitters

Rujia Zou,[a] Junqing Hu,*[a] Zhenyu Zhang,[a] Zhigang Chen[a] and Meiyong Liao[b]

Received 17th August 2010, Accepted 13th December 2010
DOI: 10.1039/c0ce00543f

Nanoribbon structures have the feature of sharp edges, providing the marked geometrical field enhancement for field emitters even in a randomly arranged thin film structure. In this work, the field emission of SnO_2 nanoribbons with thin walls (10–30 nm) prepared on a large scale *via* a rapid oxidation reaction is investigated. It is found that macroscopically, thin films made of SnO_2 nanoribbons have an extremely low electron threshold field as low as 1.23 V μm^{-1}. The SnO_2 nanoribbon field emitter also exhibits excellent emission stability, with a degradation lower than 2.7% and a huge field enhancement factor as high as 2680. Furthermore, the emission current decrease slightly, while the stability remains excellent even for a poor vacuum of 10^{-4} Pa. These field emission properties of the present SnO_2 nanoribbons surpass any other reported SnO_2 nanostructures. This work opens the avenues for SnO_2 nanoribbon structures as promising thin film field emitters.

Introduction

Tin dioxide, SnO_2, is an n-type semiconductor with a wide band gap (E_g = 3.6 eV, at 300 K) and well-known for its potential applications in gas sensors, dye-based solar cells, transparent conducting electrodes, and catalyst supports.[1–4] Because of one-dimensional (1D) nanostructures possessing remarkable properties compared to the corresponding bulk materials, the examination of the desired properties from the nanostructures for practical applications has stimulated great enthusiasm. Among these properties, field emission (FE) based on 1D nanostructures, such as carbon nanotubes,[5] CN nanotubes,[6] SiC nanowires,[7] ZnO nanorods,[8] W nanowires,[9] and so forth, has attracted prime interest due to potential applications in flat panel displays. Generally, fairly high emission current density, *i.e.*, 10 mA cm^{-2}, is desirable to light a phosphor display. Electron emission from carbon nanotubes and other inorganic nanowires/nanorods has mainly been attributed to their tips with high aspect ratio; thus, aligned growth should fashion a high-current emission due to efficiently increased number of active emitter per unit area. In contrast to nanotubes having a cylinder geometry, nanobelts exhibit distinct rectangular cross sections and large field emission area, and, therefore, have sharp corners and edges. Keeping in mind that size and shape control is a crucial factor in determining the properties of a given nanomaterial with respect to its specific applications, the study on field-emission behaviour of nanobelts is of great interest both from scientific and technological points of view. Moreover, the geometries of nanobelts can be manufactured into emitter devices more simply than the shapes of nanotubes and nanowires/nanorods, because the nanobelts are not needed to be oriented perpendicularly on substrate materials. Previous studies on the FE properties of the SnO_2 nanostructures revealed that they had high threshold field and poor emission stability.[10–12] For example, the threshold field from beaklike SnO_2 nanorods was higher than 4.4 V μm^{-1}, and field enhancement factor of these structures was lower than 1500.[10] Therefore, the search of SnO_2 material possessing excellent field emission properties has recently received considerable attention.

In this work, field emission properties from SnO_2 nanoribbons, which were prepared in large scale *via* a rapid oxidation reaction have been investigated. However, the FE from the SnO_2 nanoribbon thin films has been investigated to be show poor FE properties.[13,14] It is observed that they can operate at a low threshold field of 1.23 V μm^{-1}, and possess long-time emission stability under a constant applied voltage, which are important for the applications as electron-emitting sources in various electronic devices. In fact, the field emission properties of the present SnO_2 materials are much better than any other reported SnO_2 nanostructured and even other promising inorganic semiconductor materials. Therefore, as-fabricated SnO_2 nanoribbons could act as stronger electron emitters in electronic devices.

Experimental

The SnO_2 nanoribbons were synthesized through thermal oxidation reaction using a mixture of elemental Sn and $Fe(NO_3)_3$ as source materials in a horizontal high-temperature resistance alumina tube furnace with a copper cold finger, as described in detail elsewhere.[15] A mixture of elemental tin (3 g, 100 mesh, 99.5%) and $Fe(NO_3)_3$ (5 g, 98%) powders was placed on an

[a]*State Key Laboratory for Modification of Chemical Fibers and Polymer Materials, College of Materials Science and Engineering, Donghua University, Shanghai, 201620, China. E-mail: hu.junqing@dhu.edu.cn*
[b]*Sensor Materials Center, National Institute for Materials Science (NIMS), 1-1 Namiki, Tsukuba, Ibaraki, 305-0044, Japan*

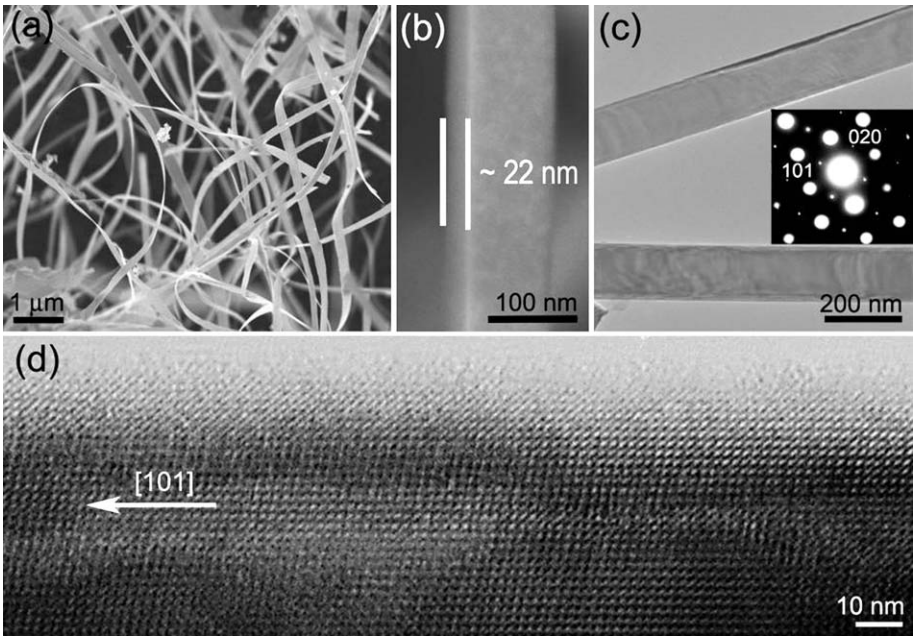

Fig. 1 (a) SEM images of the SnO_2 nanoribbons. (b) High-magnification SEM image of the SnO_2 nanoribbon. (c) TEM image of a single SnO_2 nanoribbon; the inset showing the SAED pattern along the [001] axis. (d) HRTEM image of the nanoribbon with [110] growth direction.

alumina wafer. After transferring the wafer to the center of the alumina tube, the tube was evacuated by a mechanical rotary pump to a pressure of 6×10^{-2} Torr. During the experiment, a constant flow of Ar mixed with 5% H_2 was maintained at a flow rate of 50 sccm, and the pump continually evacuated the system so that the pressure inside the tube was kept at 350 Torr. The temperature of the furnace was increased to 800 °C from room temperature and kept at 800 °C for 30 min and then further increased to 1080 °C for 30 min. After the furnace was cooled to room temperature, a white wool-like product was formed on the inner wall of the tube near the cooling finger. The yield of the products was so high (20–30%, according to the amount of tin used) that the alumina tube was clogged with as-synthesized materials after a growth period of 30 min.

Results and discussion

Scanning electron microscopy (SEM) image shows that as-synthesized products consist of a large quantity of straight and twisted nanoribbons, as shown in Fig. 1(a); the lengths of the ribbons were up to several hundreds of micrometres, even to the scale of millimetre. The high-magnification SEM image in Fig. 1(b) reveals that this nanoribbon (marked by two parallel lines) has a thickness of about 10–30 nm. Transmission electron microscopy (TEM) images in Fig. 1(c) reveals that each ribbon has a uniform width and thickness along its entire length, and the typical width is in the range of 30–160 nm. The insetting selected area electron diffraction (SAED) pattern of the ribbon in Fig. 1(c) was recorded with the electron beam along the [001] zone axis. A high-resolution TEM (HRTEM) image (Fig. 1(d)) taken from the ribbon confirmed that the single-crystal ribbon grew along the [110] direction (indicated with an arrow). As seen from the image, this ribbon is a structurally-uniform single crystal, and no dislocations or other planar defects are observed within it. The edge of the ribbon is clean and very abrupt on an atomic scale, and there are no amorphous layers covering the surface.

Our field emission experiments of the SnO_2 nanoribbons films were performed using a sphere-to-plane technique with a separated distance between the anode and cathode, and applying an optical bending beam method.[16] The threshold field is defined as the macroscopic electric field where an emission current of 1 nA is reached.[17] Typically, the sample is bent using a glass fiber placed in the middle of the sample, in which two glass slides are used to clip down both ends of the sample and create a curvature, as schematically shown Fig. 2. It has proven that this method can obtain exact data for these films samples in the field emission experiments. Different sizes (from 10.06 to 10.17 mm) are used, which allows for different compressive stresses to be applied onto the SnO_2 nanoribbon films. A direct current (dc) voltage, increasing from 100 to 800 V, was applied to SnO_2 nanoribbon thin films used as a cathode-sample in a high vacuum chamber with a base pressure of $\sim 2 \times 10^{-7}$ Pa. Fig. 3(a) shows a typical FE current as a function of the voltage of the SnO_2 nanoribbon thin film. The emission characteristics are frequently analyzed using the Fowler–Nordheim (F–N) theory,[18,19] which has proven to be useful for describing the field emission from electron emitters made of different materials. The emission current density can be represented by the following F–N equation: $I = aV^2 \exp\left(-\frac{b}{V}\right)$, $b = \frac{0.95B\phi^{3/2}}{\beta'}$, where β' is the local field

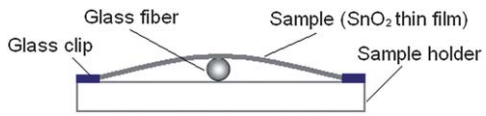

Fig. 2 A schematic diagram of the experimental configuration for field emission measurements.

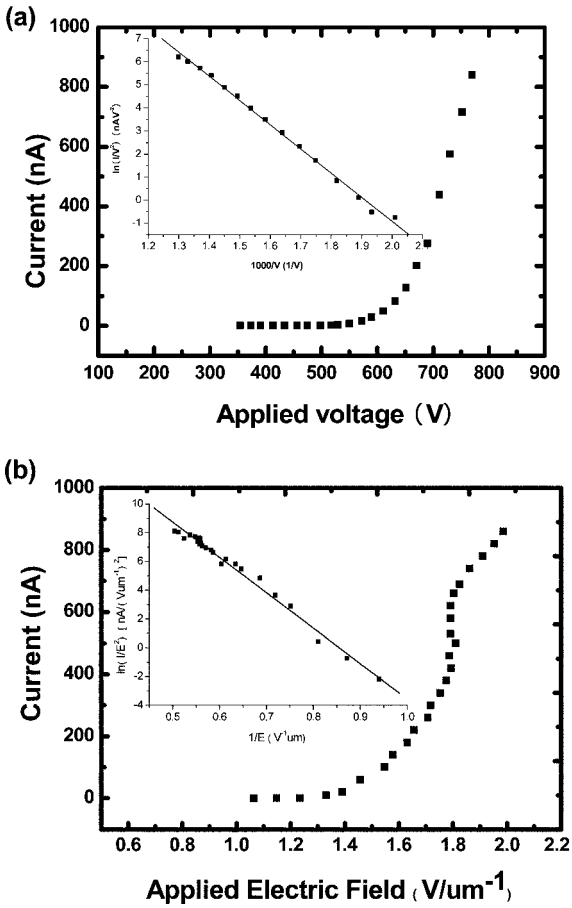

Fig. 3 (a) Field emission current *vs.* voltage (*I–V*) characteristics of the SnO_2 nanoribbon thin films; the inset shows the corresponding F–N plot. (b) Field emission current *vs.* electric field (*I–E*) characteristics of the SnO_2 nanoribbon thin films; the inset shows the corresponding F–N plot.

conversion factor at the emitting surface, a is a constant, $B = 6.87 \times 10^7$, and Φ is work function value of 4.75 eV for SnO_2.[20] The electric field enhancement factor β can be estimated from the local field (E_{loc}) equation: $E_{loc} = \frac{\beta V}{d}$, where, d is the distance between the anode and the cathode. Combining these relationship gives $\beta = \frac{0.95B\phi^{3/2}d}{b}$, where b is the slope of the F–N plot. Generally, the F–N curve is composed of straight lines separated by these corresponding applied electric fields, as shown in inset in Fig. 3(a). This implies that present field emission from SnO_2 nanoribbon thin films follows the F–N theory. In order to precisely obtain the field emission current as a function of electric field, we measured the current–voltage from SnO_2 nanoribbon thin films at various anode locations with a step of 0.030 mm. By analyzing the voltage dependence on the anode location, the electric field at a certain field emission current can be obtained. Fig. 3(b) shows the accurate current–electric field (*I–E*) plot of the SnO_2 nanoribbon thin film. From the *I–E* plot, the SnO_2 nanoribbon thin films have excellent threshold field value as low as 1.23 V μm^{-1}, and the emitting current is 820 nA at an applied field of 1.85 V μm^{-1}. The threshold field is greatly lower than the best value from those reported SnO_2 nanostructures (4.4 V μm^{-1});[10] even lower than those of from other nanostructures materials, such as, carbon nanotubes (1.6 V μm^{-1}),[5] needle-shape SiC (8.5 V μm^{-1}),[7] Si nanostructures (2.7 V μm^{-1}),[21] MoO_3 nanobelts (12.9 V μm^{-1}),[22] and other inorganic semiconductor nanostructures.[23] In general, FE current depends on the work function and geometry of the sample. From the slope of the $\ln(I/E^2) - 1/E$ plots, the field enhancement factor β is calculated to be about 2680 for the present SnO_2 nanoribbons. The above data has demonstrated that the SnO_2 nanoribbons possess strong FE performance. The strong field emission capability is attributed to the sharp edge of the SnO_2 nanoribbons. As is known, the field emission of the electrons also depends on the surface barrier height. Normally, an emitter which has a smaller barrier height shows better emission properties than that with a larger emission barrier height. Thus intensive electrons can be emitted easily even if a small voltage is applied, *i.e.*, a high emission current can be obtained at a very low voltage. In fact, the surface state of a given material is an important factor influencing the surface barrier height. In present case, as suggested by TEM imaging, SnO_2 nanoribbons are a structurally-uniform single crystal, and no dislocations or other planar defects exists within them; the surfaces of the SnO_2 nanoribbons are very clean, and there are no amorphous layers covering them. These facts also favour the easy emission of the SnO_2 nanoribbons. In fact, these arguments have been confirmed by other materials. For an example, Ren *et al.*[24] have demonstrated that the FE properties of ZnO nanobelts can be significantly enhanced by increasing the field-enhancement factor *via* either changing the geometry configuration or increasing the nanobelt field area. We observe a similar phenomenon: the excellent FE properties could be achieved through increasing the geometry configuration of the SnO_2 nanobelts; the length of the present SnO_2 nanoribbons is up to several tens of micrometres and their thickness is in the range of tens of nanometres. In a word, the thin wall nature, along with the perfect crystal structure and clean surfaces of the SnO_2 nanoribbons leads to improved field emission.

The field emission stability of the SnO_2 nanoribbons was also measured. Fig. 4 illustrates the typical fluctuation of the field emitting current for SnO_2 nanoribbon thin films, which were recorded continually at 789 V for 7000 s (at 2×10^{-7} Pa). It is found that the fluctuation of the field emitting current is low of the total emitting current during an extraordinarily long time. Significantly, there is no remarkable degradation of the emission

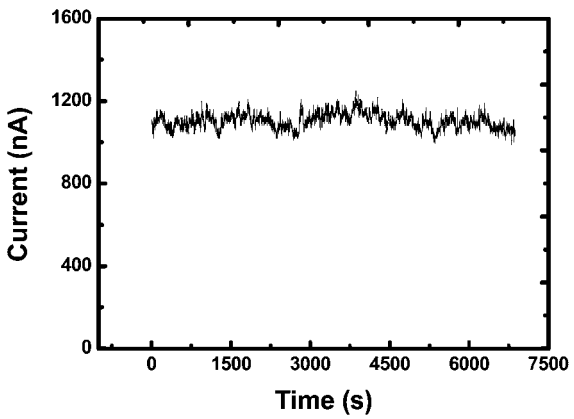

Fig. 4 The typical emission stability at constant electric field of 789 V.

current in this whole testing time or even more long time; the degradation rate from the first 10 min to the last 10 min during this testing time is lower than 2.7%. To our best knowledge, there are few reports that SnO_2 nanostructures have so long time emission stability. Therefore, it is concluded that the present SnO_2 nanoribbons displayed extremely good emission stability.

The base pressure influence on the field emission properties of the SnO_2 nanoribbons were also investigated, which is technologically required for practical applications. As shown in Fig. 5(a), at a certain voltage with the same anode-cathode distance, a slight decrease of the emission current was observed as the base pressure increases from 2×10^{-7} Pa to 1.1×10^{-4} Pa. To examine the origin for the reduction of the emission current, the field emission *I–V* characteristics were measured under the same conditions except of the base pressure, as shown in Fig. 5(b). These two *I–V* characteristics were analyzed by F–N theory, as inserted in Fig. 5(b). It was found the slope of the F–N plot at 1.1×10^{-4} Pa decreased by 1.12 times when compared to that of at 2×10^{-7} Pa. The decrease of the emission current is greatly lower than the best value from carbon nanotubes.[25,26] Since the anode-cathode arrangement did not change during the changing of the pressure, we assume that the geometrical enhancement factor and the emission area are the same for these two pressures. Therefore, the slight decrease of the field emission current at higher pressure is explained by the slight increase of the surface barrier height. Such an assumption is also supported by the intercept difference of the F–N plots at different pressure. Therefore, the vacuum state influences the field emission properties, however, slightly. For a measurement system with a poor vacuum, the electrons emitted from SnO_2 nanoribbons will interact with the gas molecules inside the vacuum. As a result, a part of these gas molecules will be ionized (by gas-phase electron ionization or by ion desorption from the anode or induced by the emitted electrons) inside the vacuum system. However, the ion bombardment seems trivial for the vacuum of 10^{-4} Pa from the emission stability data shown in Fig. 5(a). On the other hand, in a low vacuum, the emitter surface is generally contaminated by the absorption of residual gas molecules. The change of the emission barrier height as a consequence of absorption is given by an equation:[27,28] $\Delta\phi = \frac{N_s P_i \theta}{\varepsilon_0}$, where N_s is the quantity of adsorption sites per area (m^{-2}), P_i is the dipole moment per adsorbed particle (m), θ is the fractional coverage, and ε_0 is the permittivity of the vacuum. For a given material with non-uniform structure and unclean surfaces, the residual gas molecules have a large P_i and a small ε_0 in a low vacuum, contributing significantly to the poor field emission properties. In the present case, the residual gas absorption is deduced to change the work function of the SnO_2 nanoribbon slightly. This is reasonable considering that SnO_2 is a gas sensitive material. However, the experimental data reveals that the SnO_2 nanoribbons still exhibit excellent field emission properties even for a poor vacuum of 10^{-4} Pa. In CNTs emission emitter, the CNTs exhibit a fast degradation of the emission current field in a poor vacuum. It is due to that the small diameter tubes are easily destroyed, either by ion bombardment (from gas-phase electron ionization) or by ion desorption from the anode, both induced by the emitted electrons).[25] However, in our experimental, we found that after the field emission measurement no any obvious changes of the sharp edges from the SnO_2 nanoribbons were observed by TEM imaging. The excellent field emission stability is also attributed to the sharp edge of the SnO_2 nanoribbons. Therefore, the SnO_2 nanoribbons could serve as highly valuable candidates for the applications as excellent field-emitters.

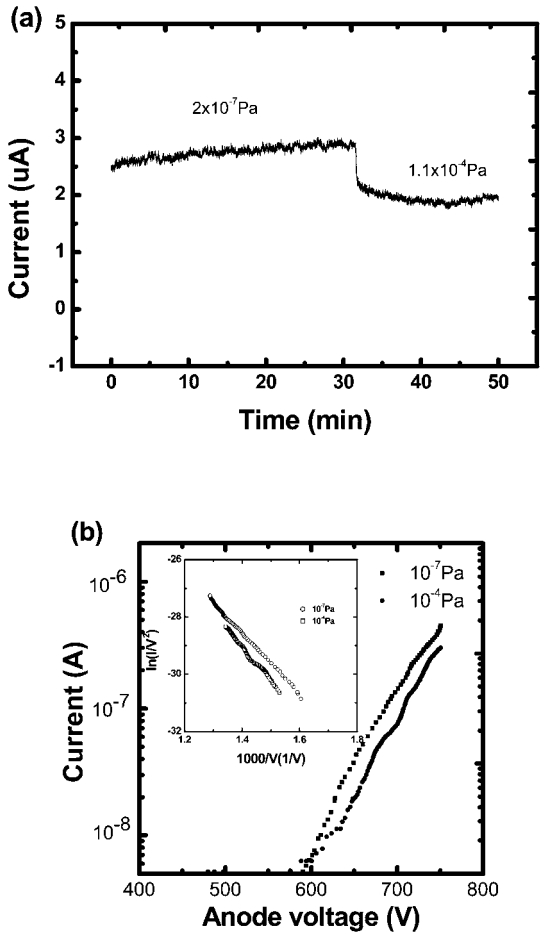

Fig. 5 (a) Long-term field emission stability of SnO_2 nanoribbons at different vacuums and constant voltages. (b) Field emission current *vs.* electric field (*I–V*) characteristics of the SnO_2 nanoribbon thin films at different vacuums and constant voltages; the inset shows the corresponding F–N plot.

Conclusions

In conclusion, field emission properties from SnO_2 nanoribbons, which were prepared in large scale *via* a rapid oxidation reaction have been investigated. These nanoribbons show strong field emission properties because they exhibit distinct rectangular cross sections, large field emission areas, and sharp corners and edges. The macroscopically thin films made of the present SnO_2 nanoribbons have extremely low electron threshold field and excellent emission stability: the threshold field is as low as 1.23 V μm^{-1}, and emitting current is 820 nA under the condition of 1.85 V μm^{-1}, and the degradation of the emission current in an extraordinarily long time (>7000 s) is lower than 2.7%, while the field enhancement factor is higher than 2680. Even for a vacuum of 10^{-4}Pa, the emission current of the SnO_2 nanoribbons

decreases slightly while keeping a good stability. There field emission properties are greatly better than any other reported SnO_2 nanostructures, and even those of the promising nanostructured inorganic semiconductor materials. Therefore, as-fabricated SnO_2 nanoribbons could serve as highly valuable candidates for the applications as electron-emitting sources in various electronic devices.

Acknowledgements

This work was supported from the National Natural Science Foundation of China (Grant No. 50872020 and 50902021), the Program for New Century Excellent Talents of the University in China, the "Pujiang" Program of Shanghai Education Commission (Grant No. 09P51400500), the "Dawn" Program of the Shanghai Education Commission (Grant No. 08SG32), the Shanghai Leading Academic Discipline Project (Grant No. B603), the Science and Technology Commission of Shanghai-based "Innovation Action Plan" Project (Grant No. 10JC1400100), the "Chen Guang" project (Grant No. 09CG27) supported by the Shanghai Municipal Education Commission and Shanghai Education Development Foundation, the Program for the Specially Appointed Professor by Donghua University (Shanghai, P. R. China), the Program of Introducing Talents of Discipline to Universities (No. 111-2-04), and the Innovation Foundation of DHU for PhD Graduates (No. BC20101224).

References

1 S. G. Ansari, P. Boroojerdian, S. R. Sainkar, R. N. Karekar, R. C. Alyer and S. K. Kulkarni, *Thin Solid Films*, 1997, **295**, 271.
2 S. Ferrere, A. Zaban and B. A. Gsegg, *J. Phys. Chem. B*, 1997, **101**, 4490.
3 Y. S. He, J. C. Campbell, R. C. Murphy, M. F. Arendt and J. S. Swinnea, *J. Mater. Res.*, 1993, **8**, 3131.
4 W. Dazhi, W. Shulin, C. Jun, Z. Suyuan and L. Fangqing, *Phys. Rev. B: Condens. Matter*, 1994, **49**, 14282.
5 M. Sveningsson, R. E. Morjan, O. A. Nerushev, Y. Sato, J. Bäckström, E. E. B. Campbell and F. Rohmund, *Appl. Phys. A: Mater. Sci. Process.*, 2001, **73**, 409.
6 D. Golberg, P. S. Dorozhkin, Y. Bando, Z. C. Dong, C. C. Tang, Y. Uemura, N. Grobert, M. Reyes-Reyes, H. Terrones and M. Terrones, *Appl. Phys. A: Mater. Sci. Process.*, 2003, **76**, 499.
7 J. Yu, E. G. Wang and X. D. Bai, *Appl. Phys. Lett.*, 2001, **78**, 2226.
8 Q. Zhao, X. Y. Xu, X. F. Song, X. Z. Zhang, D. P. Yu, C. P. Li and L. Guo, *Appl. Phys. Lett.*, 2006, **88**, 033102.
9 Y. H. Lee, C. H. Choi, Y. T. Jang, E. K. Kim, B. K. Ju, N. K. Min and J. H. Ahn, *Appl. Phys. Lett.*, 2002, **81**, 745.
10 J. H. He, T. H. Wu, C. L. Hsin, K. M. Li, L. J. Chen, Y. L. Chueh, L. J. Chou and Z. L. Wang, *Small*, 2006, **2**, 116.
11 L. A. Ma and T. L. Guo, *Phys. B*, 2008, **403**, 3410.
12 J. Wu, K. Yu, L. J. Li, J. W. Xu, D. J. Shang, Y. E. Xu and Z. Q. Zhu, *J. Phys. D: Appl. Phys.*, 2008, **41**, 185302.
13 Y. J. Chen, Q. H. Li, Y. X. Liang, T. H. Wang, Q. Zhao and D. P. Yu, *Appl. Phys. Lett.*, 2004, **85**, 5682.
14 L. J. Li, K. Yu, H. B. Mao and Z. Q. Zhu, *Appl. Phys. A: Mater. Sci. Process.*, 2010, **99**, 865.
15 J. Q. Hu, X. L. Ma, N. G. Shang, Z. Y. Xie, N. B. Wong, C. S. Lee and S. T. Lee, *J. Phys. Chem. B*, 2002, **106**, 3823.
16 R. G. Lacerda, P. Hammer, C. M. Lepienski, F. Alvarez and F. C. Marques, *J. Vac. Sci. Technol., A*, 2001, **19**, 971.
17 C. H. P. Poak, S. R. P. Silva, G. A. J. Amaratunga, W. I. Milne and F. C. Marques, *Appl. Phys. Lett.*, 2005, **86**, 232102.
18 C. A. Spindt, I. Brodie, L. Humphrey and E. R. Westerberg, *J. Appl. Phys.*, 1976, **47**, 5248.
19 R. J. Zou, J. Q. Hu, Y. L. Song, N. Wang, H. H. Chen, H. H. Chen, J. H. Wu, Y. G. Sun and Z. G. Chen, *J. Nanosci. Nanotechnol.*, 2010, **10**, 7876.
20 M. N. Islam and M. O. Hakim, *J. Mater. Sci. Lett.*, 1986, **5**, 63.
21 Z. W. Pan, H. L. Lai, F. C. K. Au, X. F. Duan, W. Y. Zhou, W. S. Shi, N. Wang, C. S. Lee, N. B. Wong, S. T. Lee and S. S. Xie, *Adv. Mater.*, 2000, **12**, 1186.
22 Y. B. Li, Y. Bando, D. Golberg and K. Kurashima, *Appl. Phys. Lett.*, 2002, **81**, 5048.
23 X. S. Fang, Y. S. Bando, U. K. Gautam, C. H. Ye and D. Golberg, *J. Mater. Chem.*, 2008, **18**, 509.
24 S. H. Jo, D. Banerjee and Z. F. Ren, *Appl. Phys. Lett.*, 2004, **85**, 1407.
25 J. M. Bonard, F. Maier, T. Stökli, A. Chatelain, W. A. de Heer, J. P. Salvetat and L. Forro, *Ultramicroscopy*, 1998, **73**, 7.
26 J. M. Bonard, J. P. Salvetat, T. Stökli, W. A. de Heer, L. Forró and A. Chatelain, *Appl. Phys. Lett.*, 1998, **73**, 918.
27 A. J. Emons and K. L. Hagemans, *J. Vac. Sci. Technol.*, 1972, **9**, 112.
28 M. Nagao, T. Kondo, Y. Gotoh, H. Tsuji, J. Ishikawa, K. Miyata and K. Kobashi, *Jpn. J. Appl. Phys.*, 1997, **36**, L1250.